....

Electric-field control of ferromagnetism

H. Ohno, D. Chiba, F. Matsukura, T. Omiya, E. Abe, T. Dietl*, Y. Ohno & K. Ohtani

Laboratory for Electronic Intelligent Systems, Research Institute of Electrical Communication, Tohoku University, Katahira 2-1-1, Aoba-ku, Sendai 980-8577, Japan
* Present address: Institute of Physics and College of Science, Polish Academy of Sciences, al. Lotników 32/46, PL-02668 Warszawa, Poland

....

It is often assumed that it is not possible to alter the properties of magnetic materials once they have been prepared and put into use. For example, although magnetic materials are used in information technology to store trillions of bits (in the form of magnetization directions established by applying external magnetic fields), the properties of the magnetic medium itself remain unchanged on magnetization reversal. The ability to externally control the properties of magnetic materials would be highly desirable from fundamental and technological viewpoints, particularly in view of recent developments in magnetoelectronics and spintronics[1,2]. In semiconductors, the conductivity can be varied by applying an electric field, but the electrical manipulation of magnetism has proved elusive. Here we demonstrate electric-field control of ferromagnetism in a thin-film semiconducting alloy, using an insulating-gate field-effect transistor structure. By applying electric fields, we are able to vary isothermally and reversibly the transition temperature of hole-induced ferromagnetism.

(In,Mn)As, used as the magnetic channel material, is one of the ferromagnetic III–V semiconductors[3–6] and is chosen for the following two reasons: (1) it exhibits hole-induced ferromagnetism (transition temperature $T_C \approx 30$ K or below)[3,4] and photo-carrier-induced magnetic transitions[7] at relatively low carrier concentration, which is important for the gate control of carrier concentration; and (2) it can be epitaxially grown within non-magnetic semiconducting InAs/(Al,Ga)Sb heterostructures, thereby allowing precise control of nonmagnetic–magnetic structures. Manganese substitutes indium in (In,Mn)As[8,9] and simultaneously provides a localized magnetic moment and a hole, owing to its acceptor nature. These holes mediate magnetic interaction, resulting in ferromagnetism[10]. Because a weak antiferromagnetism caused by superexchange is observed in the absence of holes[11], the decrease (increase) of the hole concentration by the application of electric

fields is expected to result in a reduction (an increase) of the hole-mediated ferromagnetic exchange interaction among localized Mn spins, and hence in the modification of ferromagnetic properties as shown in Fig. 1, in the cross-section of the metal-insulator–semiconductor field-effect transistor (FET) structure studied here.

The semiconductor structure consists of, from the surface side, 5 nm of (In,Mn)As (with Mn composition 0.03), 10 nm of InAs, 400 nm of (Al,Ga)Sb (with Al composition 0.6) and 100 nm of AlSb on semi-insulating (001) GaAs substrates. The AlSb and (Al,Ga)Sb layers serve as a buffer structure, in which most of the 7% lattice-mismatch between the GaAs substrate and the epitaxial layers is relaxed. The thin InAs buffer layer ensures the two-dimensional growth of the subsequent (In,Mn)As layer and improves its magnetic quality[12]. All the layers are grown by solid-source molecular beam epitaxy; the AlSb and (Al,Ga)Sb layers are grown at 550 °C, the InAs layer at 450 °C, and the magnetic layer at 250 °C. A Hall bar geometry mesa is first formed by Cl dry-etch removal of the unwanted epitaxial layers. Then a 0.8-μm thick polyimide layer (relative dielectric constant 3.3) is spun-on, which acts as a gate insulator, and contact holes for source and drain are formed. Finally, the Cr(5 nm)/Au(95 nm) gate electrode is defined by a lift-off process and the source and drain contacts are made by indium bonding. The gate leakage currents are less than 5 nA cm^{-2} in all the devices. The potential probes of the Hall bar are separated by 80 μm and the width of the channel is 60 μm. Below, we show typical results obtained from over 40 FETs fabricated thus far.

The small dimension of the device together with the thick diamagnetic GaAs substrate makes it difficult to measure directly the magnetization of the magnetic layer. We use the magnetization-dependent Hall effect to extract the magnetic properties of the channel layer. The sheet Hall resistivity, R_{Hall}, is given by the sum of the ordinary Hall effect due to the Lorenz force and the anomalous Hall effect originating from the asymmetric scattering in the presence of magnetization:

$$R_{Hall} = \frac{R_0}{d}B + \frac{R_S}{d}M$$

where R_0 is the ordinary Hall coefficient, B and M the magnetic field and the magnetization perpendicular to the layer, respectively, R_S the anomalous Hall coefficient, and d the thickness of the channel
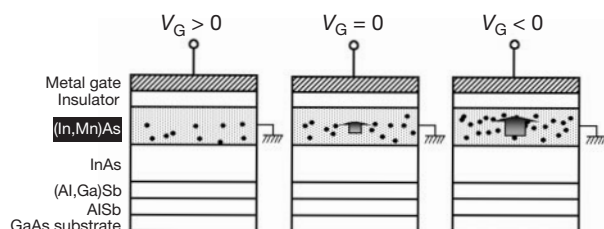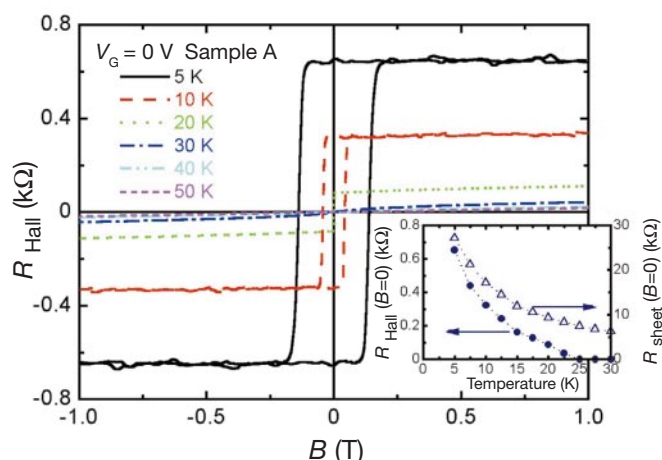

Figure 1 Field-effect control of the hole-induced ferromagnetism in magnetic semiconductor (In,Mn)As field-effect transistors. Shown are the cross-sections of a metal-insulator–semiconductor structure under gate biases V_G. This controls the hole concentration in the magnetic semiconductor channel (filled circles). Negative V_G increases hole concentration, resulting in enhancement of the ferromagnetic interaction among magnetic Mn ions, whereas positive V_G has an opposite effect. The arrow schematically shows the magnitude of the Mn magnetization. The InAs/(Al,Ga)Sb/AlSb structure under the (In,Mn)As layer serves as a buffer relaxing the lattice mismatch between the structure and the GaAs substrate to produce a smooth surface on which the magnetic layer is grown.

Figure 2 Magnetic-field dependence of the sheet Hall resistance R_{Hall} proportional to the magnetization of the magnetic semiconductor layer. R_{Hall} is used to measure the small magnetization of the channel. Shown are R_{Hall} as a function of field perpendicular to the layer at temperatures $T = 5$–50 K of sample A at $V_G = 0$ V. Clear hysteresis observed at $T \lesssim 20$ K is evidence of ferromagnetism. Inset, the temperature dependence of the remanence of R_{Hall} (solid circles), showing that the ferromagnetic transition temperature T_C is above 20 K. Open circles indicate the channel sheet resistance R_{sheet} at zero field, which shows moderate negative T-dependence.

layer[13]. R_S is proportional to ρ^γ, where ρ is the resistivity of (In,Mn)As. Normally γ is either 1 or 2 (ref. 13). The R_{Hall} versus B curves of sample A with the gate bias $V_G = 0$ V are shown in Fig. 2. The clear square hysteresis at low temperatures $T \lesssim 20$ K shows that the (In,Mn)As layer is ferromagnetic with perpendicular easy axis[4] and $R_{Hall} \propto M$, enabling us to extract the magnetization of the channel layer. At room temperature, the ordinary Hall effect dominates because of the much reduced susceptibility of the channel. Temperature dependence of the remanence in R_{Hall} (R_{Hall} at $B = 0$ T) shown in the inset indicates that T_C is above 20 K (T_C varies by about 20% from device to device). The inset also shows that the channel sheet resistance R_{sheet} at $B = 0$ T gradually increases as temperature decreases. In the following experiments, we apply $V_G = \pm 125$ V, which modulates ± 4–6% of R_{sheet} in the range of $T = 5$–300 K. From the gate capacitance, $|V_G| = 125$ V is expected to produce a sheet hole concentration change of 3×10^{12} cm^{-2}; hence, assuming a constant mobility, the total sheet hole concentration is 5–8 $\times 10^{13}$ cm^{-2}, in agreement with the Hall concentration at 300 K.

The R_{Hall} versus B near T_C at $T = 22.5$ K of sample B under three different V_G measured in the sequence of $V_G = 0$, +125, −125 and 0 V are displayed in Fig. 3. The measurements are done with a small constant current flow, where no current dependence is present. At $V_G = 0$ V, a moderate hysteresis is observed in the curve, confirming that the sample temperature is close to but below T_C. Application of $V_G = +125$ V (in the direction of depletion of holes) transforms the moderate hysteresis loop to a paramagnetic response with reduced susceptibility and no hysteresis. Switching V_G to −125 V changes the response to the one with a clear square hysteresis. The original R_{Hall}−B curve is restored when V_G is returned to 0 V. The inset shows the same curves to higher magnetic fields. The qualitative difference of the magnetization curves obtained in Fig. 3 indicates that the magnetism of the channel layer is modified isothermally in a reversible way by the external gate voltage.

Figure 4 shows the spontaneous R_{Hall} (R_{Hall}^S), which is proportional to the spontaneous magnetization M_S, around T_C of sample A under the three gate biases ($V_G = +125$, 0, and −125 V). Because T_C is the temperature at which M_S (and hence R_{Hall}^S) becomes zero, Fig. 4

clearly shows that the applied gate bias changes T_C by ± 1 K ($\Delta T_C / T_C = \pm 4\%$), and in this temperature range, ferromagnetism can be turned on and off by the external electric fields. R_{Hall}^S, shown in Fig. 4, is determined from the extrapolation of R_{Hall} from the moderate fields ($0.1 < B < 0.7$ T) to $B = 0$ using an Arrott plot to minimize the effects of domain wall formation and magnetic anisotropy[14]. The inset of Fig. 4 shows the typical Arrott plots of sample A near T_C, where the intercept of a linear extrapolation of R_{Hall}^2 at $B = 0$ gives $(R_{Hall}^S)^2$. A negative intercept means no M_S. The narrow range of relevant temperatures and fields allows us to neglect the small T and B dependences of ρ, making the use of R_{Hall} instead of M_S an excellent approximation. The linear dependence seen in the inset shows that the contribution from the ordinary Hall effect is negligible.

Because the magnetic layer is very thin, it acts as a quantum well and V_G is believed to modulate the hole population of the two-dimensional (2D) sub-bands in the magnetic layer, as opposed to the depletion-layer movement in the three-dimensional (3D) FETs. Recent mean-field theory predicts no carrier concentration dependence of T_C for 2D systems, when only the ground sub-band with constant effective mass is occupied, because the 2D density-of-states that determines T_C is energy-independent[15]. As demonstrated in the theory for the 3D case[10], however, the realistic valence band structure including spin-orbit coupling is important to determine T_C. Because the valence band density-of-states is a complex function of energy, we expect modulation of T_C through modulation of carrier concentration even in the 2D systems. (From the 3D theory[10], we expect $\Delta T_C / T_C = 10\%$ for $\Delta p / p = 0.06$, in reasonable agreement with the present results). Additional contributions to the modulation of T_C may come from the particular design of the heterostructure employed here: a non-magnetic InAs is placed beneath the magnetic (In,Mn)As layer. Application of positive (negative) bias distorts the relevant 2D wavefunctions away from (towards) the magnetic layer, resulting in reduction (increase) of carrier–magnetic-impurity exchange interaction and hence in reduction (increase) of T_C as discussed in ref. 16.

Field-controlled ferromagnetism is expected to have a great technological impact because of the possible integration of ferromagnetic devices with non-magnetic III–V devices such as lasers
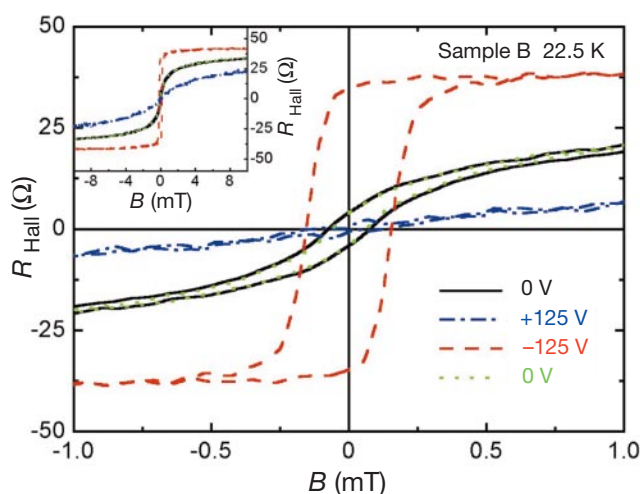

Figure 3 R_{Hall} versus field curves under three different gate biases. Application of $V_G = 0$, +125 and −125 V results in qualitatively different field dependence of R_{Hall} measured at 22.5 K (sample B). When holes are partially depleted from the channel ($V_G = +125$ V), a paramagnetic response is observed (blue dash-dotted line), whereas a clear hysteresis at low fields (<0.7 mT) appears as holes are accumulated in the channel ($V_G = -125$ V, red dashed line). Two R_{Hall} curves measured at $V_G = 0$ V before and after application of ± 125 V (black solid line and green dotted line, respectively) are virtually identical. Inset, the same curves shown at higher magnetic fields.
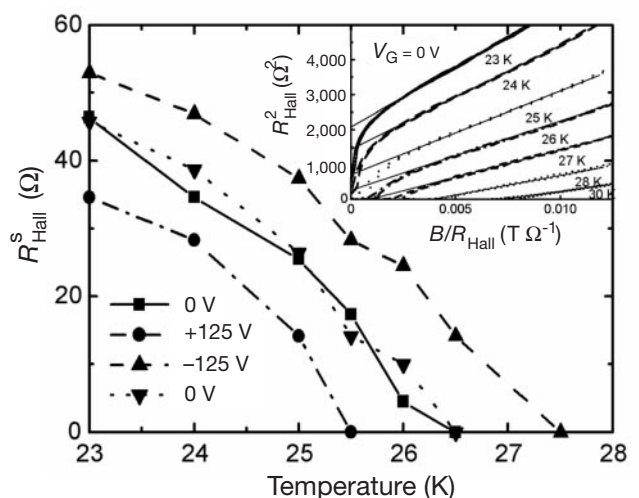
Figure 4 Temperature dependence of spontaneous Hall resistance R_{Hall}^S under three different gate biases. R_{Hall}^S proportional to the spontaneous magnetization M_S indicates ± 1 K modulation of T_C upon application of $V_G = \pm 125$ V (sample A). T_C is the temperature at which R_{Hall}^S (and hence M_S) goes to zero. Data at $V_G = 0$ V before and after application of ± 125 V are shown by squares and down triangles, respectively. In order to minimize the effect of domain rotation and magnetic anisotropy, R_{Hall}^S is determined by extrapolation of R_{Hall} from moderate fields (0.1–0.7 T) to 0 using Arrott, plots (R_{Hall}^2 versus B/R_{Hall} plots shown in inset).

 945

and transistors already in use in electronics. We note that room temperature ferromagnetism in semiconductors has been predicted[10]. Combinations of semiconductor spintronic devices[17,18] with the present field-controlled ferromagnetism may also be important in quantum information technologies that are based on manipulation of spin states in semiconductors[19,20]. ☐

1. Prinz, G. A. Magnetoelectronics. *Science* **282**, 1660–1663 (1998).
2. de Boeck, J. & Borghs, G. Magnetoelectronics. *Phys. World* **12**, 27–32 (1999).
3. Ohno, H., Munekata, H., Penney, T., von Molnár, S. & Chang, L. L. Magnetotransport properties of p-type (In,Mn)As diluted magnetic III–V semiconductors. *Phys. Rev. Lett.* **68**, 2664–2667 (1992).
4. Munekata, H., Zaslavsky, A., Fumagalli, P. & Gambino, R. J. Preparation of (In,Mn)As/(Ga,Al)Sb magnetic semiconductor heterostructures and their ferromagnetic characteristics. *Appl. Phys. Lett.* **63**, 2929–2931 (1993).
5. Ohno, H. Making nonmagnetic semiconductors ferromagnetic. *Science* **281**, 951–956 (1998).
6. Ohno, H. Properties of ferromagnetic III–V semiconductors. *J. Mag. Magn. Mater.* **200**, 110–129 (1999).
7. Koshihara, S. *et al.* Ferromagnetic order induced by photogenerated carriers in magnetic III–V semiconductor heterostructures of (In,Mn)As/GaSb. *Phys. Rev. Lett.* **78**, 4617–4620 (1997).
8. Munekata, H. *et al.* Diluted magnetic III–V semiconductors. *Phys. Rev. Lett.* **63**, 1849–1852 (1989).
9. Soo, Y. L., Huang, S. W., Ming, Z. H., Kao, Y. H. & Munekata, H. III–V diluted magnetic semiconductor: Substitutional doping of Mn in InAs. *Phys. Rev. B* **53**, 4905–4909 (1996).
10. Dietl, T., Ohno, H., Matsukura, F., Cibert, J. & Ferrand, D. Zener model description of ferromagnetism in zinc-blende magnetic semiconductors. *Science* **287**, 1019–1022 (2000).
11. von Molnár, S., Munekata, H., Ohno, H. & Chang, L. L. New diluted magnetic semiconductor based on III–V compounds. *J. Mag. Magn. Mater.* **93**, 356–364 (1991).
12. Shen, A. *et al.* Epitaxy and properties of InMnAs/AlGaSb diluted magnetic III–V semiconductor heterostructures. *Appl. Surf. Sci.* **113/114** 183–188 (1997).
13. Chien, C. L. & Westgate, C. W. *The Hall Effect and Its Applications* 43–51 (Plenum, New York, 1980).
14. Arrott, A. Criterion for ferromagnetism from observations of magnetic isotherms. *Phys. Rev.* **108**, 1394–1395 (1957).
15. Dietl, T., Haury, A. & Merle d'Aubigné, Y. Free carrier-induced ferromagnetism in structures of diluted magnetic semiconductors. *Phys. Rev. B* **55**, R3347–R3350 (1997).
16. Lee, B., Jungwirth, T. & MacDonald, A. H. Theory of ferromagnetism in diluted magnetic semiconductor quantum wells. *Phys. Rev. B* **61**, 15606–15609 (2000).
17. Fiederling, R. *et al.* Injection and detection of a spin-polarized current in a light-emitting diode. *Nature* **402**, 787–790 (1999).
18. Ohno, Y. *et al.* Electrical spin injection in a ferromagnetic semiconductor heterostructure. *Nature* **402**, 790–792 (1999).
19. Loss, D. & DiVincenzo, D. P. Quantum computation with quantum dots. *Phys. Rev. A* **57**, 120–126 (1998).
20. Vrijen, R. *et al.* Electron-spin-resonance transistors for quantum computing in silicon-germanium heterostructures. *Phys. Rev. A* **62**, 012306-1–10 (2000).

Mesoscopic fast ion conduction in nanometre-scale planar heterostructures

N. Sata, K. Eberman*, K. Eberl & J. Maier

Max-Planck-Institut für Festkörperforschung, 70569 Stuttgart, Germany

Ion conduction is of prime importance for solid-state reactions in ionic systems, and for devices such as high-temperature batteries and fuel cells, chemical filters and sensors[1,2]. Ionic conductivity in solid electrolytes can be improved by dissolving appropriate impurities into the structure or by introducing interfaces that cause the redistribution of ions in the space-charge regions[3–11]. Heterojunctions in two-phase systems should be particularly

efficient at improving ionic conduction[3,4], and a qualitatively different conductivity behaviour is expected when interface spacing is comparable to or smaller than the width of the space-charge regions in comparatively large crystals[12–15]. Here we report the preparation, by molecular-beam epitaxy, of defined hetero-layered films composed of CaF_2 and BaF_2 that exhibit ionic conductivity (parallel to the interfaces) increasing proportionally with interface density—for interfacial spacing greater than 50 nanometres. The results are in excellent agreement with semi-infinite space-charge calculations[3], assuming a redistribution of fluoride ions at the interfaces. If the spacing is reduced further, the boundary zones overlap and the predicted mesoscopic size effect[3,12] is observed. At this point, the single layers lose their individuality and an artificial ionically conducting material with anomalous transport properties is generated. Our results should lead to fundamental insight into ionic contact processes and to tailored ionic conductors of potential relevance for medium-temperature applications.

The growth of semiconductor heterostructures by molecular beam epitaxy (MBE) is the method of choice for preparing hetero-systems with highly defined geometry, periodicity, interfacial spacings and layer sequence[16,17]. We used this technique, performed in a high-vacuum chamber with a base pressure of 10^{-9} mbar. Single crystals of the moderate (anti-Frenkel disordered) fluoride conductors CaF_2 and BaF_2 (refs 18–20) were sublimed at 1,180 and 1,000 °C, respectively, leading to a layer growth rate of about 1 nm min^{-1}. Periodicity and thickness were varied over a wide range (individual layer thicknesses: 2–500 nm) by computer-controlled effusion cell shutters. The total thickness of the film packages ranged from 200 to 500 nm. Single crystals of Al_2O_3 and SiO_2 were tested as substrate materials; they showed little influence on the conductivity of the thin films, whereas they obviously affected crystallinity. The substrate was kept at a temperature of 500 °C or about 100 °C to investigate the effect of growth temperature on film structure, which could also affect the ionic conductivity.

The films were characterized by X-ray diffraction and secondary-ion mass spectrometry (SIMS). In contrast to CaF_2, the BaF_2 film grows on $Al_2O_3(012)$ substrates at a temperature of 500 °C in [111]
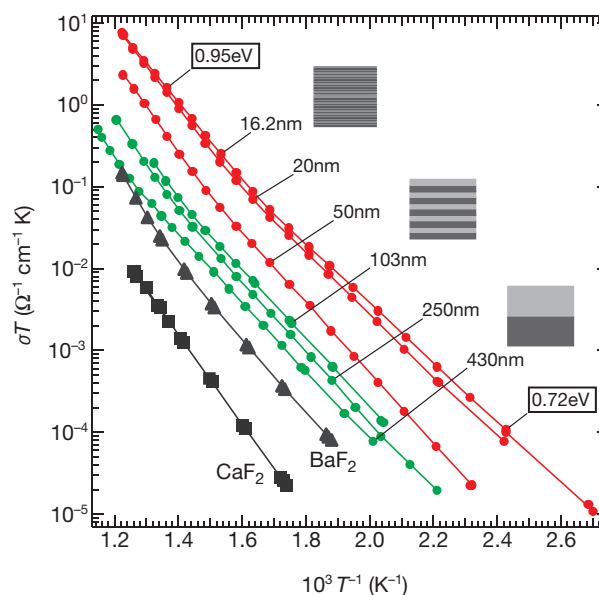

Figure 1 Parallel ionic conductivity of the films. Data are shown for films with various periods and interfacial densities in the 430–16 nm range. We note that the overall thickness is approximately the same in all cases (~500 nm). σ, conductivity; *T*, temperature. The different colours refer to different site regimes (green: semi-infinite space charge zones; red: finite space charge zones).

* Present address: 3M Center, St Paul, Minnesota 55144-1000, USA.